International Journal of Photochemistry and Photobiology
2017; 1(2): 36-43
http://www.sciencepublishinggroup.com/j/ijpp
doi: 10.11648/j.ijpp.20170102.11

Simplifying Ratiometric C-SNARF-1 pH Calibration Procedures with a Simple Post-Processing

Rutjapan Kateklum[1], Bernard Gauthier-Manuel[1], Christian Pieralli[1], Samlee Mankhetkorn[2], Bruno Wacogne[1, 3, *]

[1]FEMTO-ST Institute, UMR CNRS 6174, Université Bourgogne Franche-Comté, Besançon, France

[2]Center of Excellence in Molecular Imaging, Chiang Mai University, Chiang Mai, Thailand

[3]INSERM CIC 1431, Besançon University Hospital, Besançon, France

Email address:

rutjapan@hotmail.com (R. Kateklum), bernard.gauthier@femto-st.fr (B. Gauthier-Manuel), christian.pieralli@univ-fcomte.fr (C. Pieralli), samlee.mankhetkorn@cmu.ac.th (S. Mankhetkorn), bruno.wacogne@univ-fcomte.fr (B. Wacogne)

[*]Corresponding author

To cite this article:

Rutjapan Kateklum, Bernard Gauthier-Manuel, Christian Pieralli, Samlee Mankhetkorn, Bruno Wacogne. Simplifying Ratiometric C-SNARF-1 pH Calibration Procedures with a Simple Post-Processing. *International Journal of Photochemistry and Photobiology.* Vol. 1, No. 2, 2017, pp. 36-43. doi: 10.11648/j.ijpp.20170102.11

Received: February 23, 2017; **Accepted**: March 21, 2017; **Published**: April 14, 2017

Abstract: A simple and easy to implement numerical method is proposed in order to considerably simplify the experimental calibration procedure of C-SNARF-1 indicator used for ratiometric pH sensing. Usually, calibration is based on the measurement of fluorescence spectra using perfectly calibrated equipment at extreme pH values. The calibration solutions must be extremely well controlled in terms of indicator concentration and path length. Also, the optical equipment used must be well controlled and excitation energy as well as fluorescence collection efficiency must be perfectly constant over the whole calibration procedure. The method we propose is based on the fact that the emission fluorescence energy does not only depend on pH but also on the excitation wavelength. In this paper, we propose a model describing the evolution of the emitted energy as a function of pH and excitation wavelength. We show that the emitted energy evolves linearly with pH and we express this linear evolution as a function of the excitation wavelength. We also show the evolution of the isosbestic (or isoemitting) point as a function of the excitation wavelength. Knowing the linear dependence of the emitted energy as a function of excitation wavelength allows post-processing calibration spectra obtained with basic optical equipment where the excitation energy, fluorescence collection efficiency, indicator concentration and path length can vary over the calibration session. Because the calibration procedure becomes independent of the above mentioned parameters, the post-processing we propose considerably simplify indicators calibration. This method can easily be transposed, not only to other ratiometric pH indicators, but also to ion sensing fluorescent indicators exhibiting dual emission peaks.

Keywords: Fluorescence pH Sensing, Ratiometric Measurements, Calibration, C-SNARF-1

1. Introduction

A large number of fluorescent indicators have been developed for optical pH sensing. Initially, they have been synthetized for intracellular pH imaging [1-3], but they can also be used for other applications in optodes configurations (for example [4-7]). Two kinds of fluorescent pH indicators can be purchased. The first group includes fluorescent molecules which exhibit a single emission peak (fluorescein for example [8]). For these indicators, the fluorescence intensity is directly related to the pH of the surrounding medium. The shape of the emission spectra remains constant. Therefore, pH determination using these indicators requires normalizing the fluorescence intensity with intensity measured at high pH values (pH above 8 in reference [8]). The second group of indicators exhibits a double fluorescence emission peak. Here, each protonated or deprotonated forms exhibits characteristic fluorescence and/or absorption spectra [9]. Shifts between spectra obtained for protonated and deprotonated species can be exploited in

order to perform a ratiometric measurement. Two situations occur, either the excitation is performed at two excitation wavelengths and the fluorescence emission is measured at one wavelength, or the excitation is performed at only one excitation wavelength and fluorescence emission is measured at two emission wavelengths [10]. Under certain conditions, ratiometric measurement makes pH determination independent of the indicator concentration or optical path length because pH is related to the ratio (in excitation or emission) at two characteristic wavelengths. Despite the existence of drawbacks to using C-SNARF-1 [1, 9], this molecule and the chemical family it is belonging to has been widely used for pH sensing [11-14].

However, measuring the fluorescence emission ratio at two distinct wavelengths does not lead to an exact determination of pH. Indeed, the indicator must be calibrated using two extreme pH solutions for which ratios at measurement wavelengths are calculated. The calibration procedure can be found either in the manufacturer website [15] or in various publications [11, 16-18]. Note that the same calibration procedure can be used for general fluorescence ion concentration measurements [18-21] when dual emission peak indicators are used. Complementary calibration procedures have been proposed to take into account the biochemical variability of cells under investigation [12]. Note also that *in situ* calibration procedure can be performed using nigericin [22]. However, this method may not be applicable in all situations and it cannot be used to calibrate optodes.

The "classical" calibration procedure must be performed for various reasons listed in [10]: sensitivity of the indicator to ionic strength, specific interactions depending on the nature of the indicator or structural changes of the medium. It also requires extreme care when performing measurements as explained in [21] in the case of calcium detection. Adapted from reference [21], "any intervening loss of dye or changes in instrument sensitivity jeopardizes the calibration and may be mistaken for a change in $[H^+]$". Equation (1) presents the relationship between pH, pK_a and intensity ratios.

$$pH = pK_a - log_{10}\left[\frac{R-R_B}{R_A-R} \times \frac{I_B^2}{I_A^2}\right] \quad (1)$$

Here, R is the intensity ratio measured at wavelengths λ_1 and λ_2 for the solution of unknown pH, R_B and R_A are the intensity ratios at the same wavelengths measured for the deprotonated and protonated forms of the indicator respectively, I_A^2 and I_B^2 are the intensities measured at λ_2 for the deprotonated and protonated forms of the indicator respectively.

Consequently, extreme pH solutions must be prepared with a very controlled and reproducible indicator's concentration. The same holds for the path length in the cuvette containing the indicator. The excitation must be kept constant between low pH and high pH measurements. The collection of fluorescence must be performed with exactly the same efficiency for both measurements. These requirements may be met using laboratory level spectrofluorometers when this expensive apparatus is available, but they can be sources of experimental difficulties in other situations.

In this paper, we present a simple method to post-process calibration spectra obtained with basic optical equipment where both the excitation and fluorescence collection efficiency can differ over the calibration session. This method also allows accounting for variations of indicator's concentration or measurement path lengths. This post-processing considerably simplify indicator's calibration procedures. Indeed, calibration becomes independent of the experimental difficulties mentioned above.

2. Material and Method

The method we propose uses fluorescence spectra obtained from: the C-SNARF-1 supplier [15], the scientific literature [12, 23] and our own experimental data.

2.1. Material

1. Supplier and literature spectra were digitized using the "Engauge digitizer 3.0" freeware. They were next smoothed using the cubic spline smoothing function available in Matlab® and stored as a .txt file for subsequent numerical treatment.
2. Buffer solutions were Phosphate Buffer Saline (PBS) 0.5X composed of 68.5 mM NaCl, 5 mM phosphates (4 mM Na_2HPO_4 and KH_2PO_4 with proportion tuning the pH value), 1.35 mM KCl.
3. pHs of buffer solutions were controlled with a Hanna instrument pH211, resolution 0.01 unit pH.
4. C-SNARF-1 (serial number 1270) was purchased from Thermofisher. A stock solution was prepared adding 1 mg of indicator to 1 ml of pure water. 40 µl were sampled and added to 400 µl of water to obtained aliquots used to prepare solutions of various pHs (20µl aliquot + 1 ml buffer solution).
5. Plastic cuvettes purchased from Dominique Dutcher with 10 mm path length were filled with solutions at various pHs for fluorescence measurements.
6. Fluorescence was excited at 485 nm wavelength using an Oxxious, 488-50-COL-PP laser.
7. Excitation and emission filters as well as a dichroic mirror were integrated in a fluorescence beam-splitter purchased from Doric Lenses and equipped with collimation of injection lenses designed for multimode fibers with 200 µm diameter core. Emission filter, dichroic mirror and emission filter are FF01-488/10-25, FF500-Di01-25×36, BLP01-488-25 respectively.
8. Conventional 200 µm core optical fibers purchased from Thorlabs (M38L01) were used to connect the excitation laser to the excitation port of the fluorescence beam-splitter and the emission port of the fluorescence beam-splitter to the spectrometer.
9. Spectra were acquired with a QEP00363 spectrometer

purchased from Ocean Optics with an integration time of 100 ms. Wavelength span 348 nm to 1127 nm, 1044 pixels. No boxcar or averaging were used.

2.2. Method

The whole post-processing relies on the calculation of the energy emitted by the C-SNARF-1 for each pH and each excitation wavelength. This energy is proportional to the area under the spectra. In spectroscopy, cm^{-1} are equivalent to energy. Spectra are therefore processed in the wavenumber domain.

2.2.1. Evolution of the Fluorescence Emission Versus pH and Excitation Wavelength

Spectra used in this study are obtained by digitalization of supplier's data, data found in the literature and obtained with our own measurements. Scales of these spectra being different, spectra must be normalized so that the subsequent calculation holds for all data regardless of their origin. For each excitation wavelength, normalization consists in dividing the spectral data by the absolute maximum of spectra obtained for all pH values. This normalization can be written as follows.

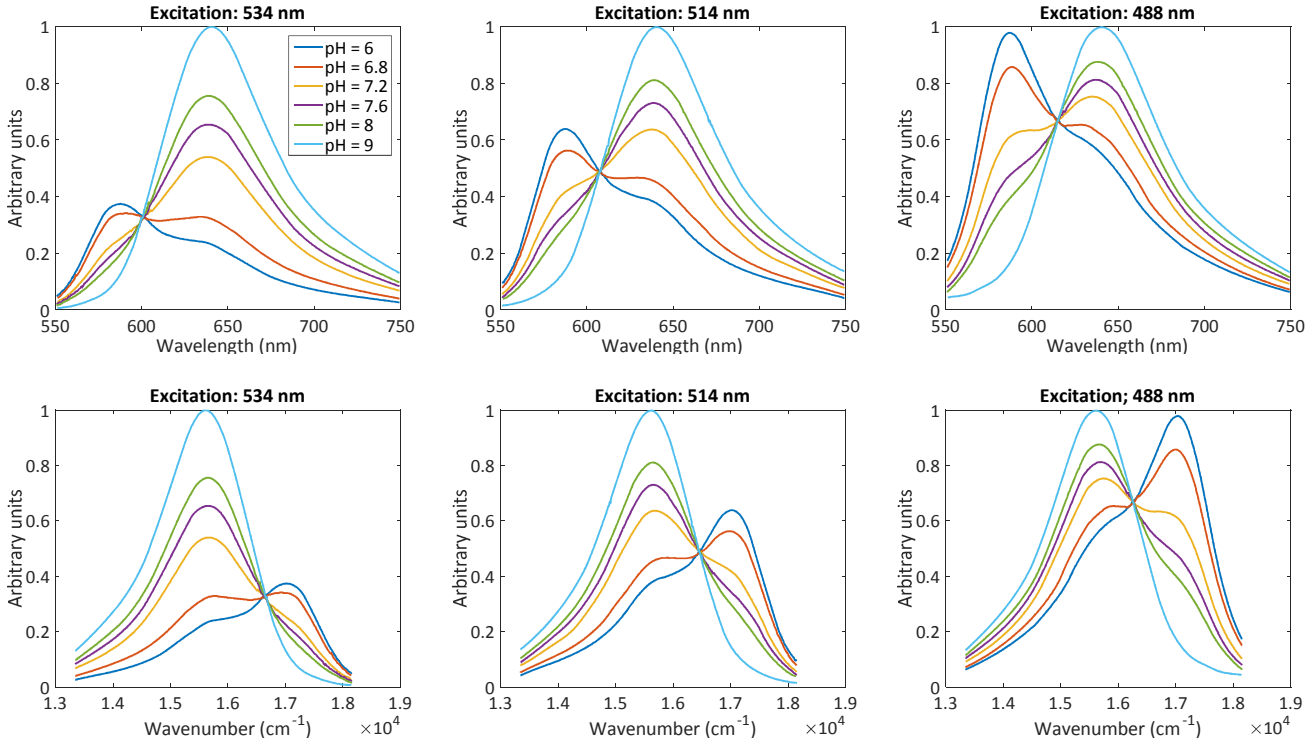

Figure 1. *Normalized emission spectra of C-SNARF-1 at different excitation wavelengths and for various pHs. Top row: spectra expressed in wavelengths. Bottom row: spectra expressed in wavenumbers. Legend indicating pHs is reproduced only once for clarity. Source [15].*

$$S_{\lambda_{ex}}^{pHi}(\lambda) \Rightarrow s_{\lambda_{ex}}^{pHi}(\sigma) \Rightarrow \tilde{s}_{\lambda_{ex}}^{pHi}(\sigma) = \frac{s_{\lambda_{ex}}^{pHi}(\sigma)}{Max\left(s_{\lambda_{ex}}^{pH1}(\sigma),\ldots,s_{\lambda_{ex}}^{pHn}(\sigma)\right)} \quad (2)$$

Here, $S_{\lambda_{ex}}^{pHi}(\lambda)$ represents spectra for an excitation at λ_{ex} at pHi expressed in wavelength, $S_{\lambda_{ex}}^{pHi}(\sigma)$ represents spectra for an excitation at λ_{ex} at pHi expressed in wavenumber and $\tilde{s}_{\lambda_{ex}}^{pHi}(\sigma)$ represents normalized spectra for an excitation at λ_{ex} at pHi expressed in wavenumbers and n the number of different pHs.

Figure 1 shows the emission spectra of C-SNARF-1 obtained from the supplier's data [15]. The top row represents spectra in wavelengths for excitation wavelength at 534 nm, 514 nm and 488 nm. The bottom row represents the same spectra expressed in wavenumbers. Note that this is only when all the above mentioned calibration parameters are perfectly controlled that an isosbestic point appears when plotting spectra.

The post-processing is based on the following observation. The area under the curves evolves according to pH. Also, this area under the curves evolves differently for different excitation wavelengths. For each spectrum, the normalized energy emitted by the indicator can be written as follows.

$$E_{\lambda_{ex}}^{pHi} = \int \tilde{s}_{\lambda_{ex}}^{pHi}(\sigma)d\sigma \quad (3)$$

As we will see in the "Results and discussion" section, for each excitation wavelength, the normalized energy evolves linearly with pH. Equation (3) can then be re-written as follows.

$$E_{\lambda_{ex}}(pH) = a_{\lambda_{ex}} \cdot pH + b_{\lambda_{ex}} \quad (4)$$

Here, $a_{\lambda_{ex}}$ and $b_{\lambda_{ex}}$ are the coefficients of the linear

evolution of the normalized energy with pH at the excitation wavelength λ_{ex}.

2.2.2. Fluorescence Spectra Post-Processing

Consider that experimental spectra, obtained with an excitation wavelength λ_{ex}, are recorded using non-perfectly controlled calibration solutions or non-perfectly controlled instrument sensitivity. Each spectrum exhibits its own energy and no isosbestic point appears when plotting the spectra.

The first step to correct these experimental spectra is to normalize them independently with their own energy (equation (5)). In this way, all normalized spectra will exhibit the same normalized energy.

$$ns_{\lambda_{ex}}^{pHi}(\sigma) = \frac{s_{\lambda_{ex}}^{pHi}(\sigma)}{\int s_{\lambda_{ex}}^{pHi}(\sigma)d\sigma} \quad (5)$$

Here, $s_{\lambda_{ex}}^{pHi}(\sigma)$ represents the experimental spectra recorded at pHi with an excitation wavelength λ_{ex} and $ns_{\lambda_{ex}}^{pHi}(\sigma)$ the normalized spectra.

Because we know the law governing the evolution of the normalized energy as a function of pH and for each excitation wavelength (equation (4)), the second step consists in calibrating the experimental spectra as follows.

$$cns_{\lambda_{ex}}^{pHi}(\sigma) = \frac{s_{\lambda_{ex}}^{pHi}(\sigma)}{\int s_{\lambda_{ex}}^{pHi}(\sigma)d\sigma} \cdot \left(a_{\lambda_{ex}} \cdot pH + b_{\lambda_{ex}}\right) \quad (6)$$

Here, $cns_{\lambda_{ex}}^{pHi}(\sigma)$ represents the corrected experimental spectra recorded at pHi for an excitation wavelength λ_{ex}. As we will see in the "Results and discussion" section, spectra are correctly corrected and the isosbestic point appears clearly. The calibration procedure can now be performed because the ratios R, R_B and R_A as well as the ratio I_B^2/I_A^2 can be calculated precisely using the re-calibrated spectra.

An extreme control of the calibration experimental parameters is not required anymore.

2.2.3. Linear Coefficients and Isosbestic Point as a Function of the Excitation Wavelength

As it will be shown in the next section, linear coefficients $a_{\lambda_{ex}}$ and $b_{\lambda_{ex}}$ as well as the position of the isosbestic point IB linearly depend on λ_{ex}. These behaviors are given as follows.

$$\begin{aligned} a_{\lambda_{ex}}(\lambda_{ex}) &= \alpha_1 \cdot \lambda_{ex} + \alpha_2 \\ b_{\lambda_{ex}}(\lambda_{ex}) &= \beta_1 \cdot \lambda_{ex} + \beta_2 \end{aligned} \quad \text{for the linear coefficients} \quad (7)$$

$$IB(\lambda_{ex}) = \gamma_1 \cdot \lambda_{ex} + \gamma_2 \quad \text{for the isosbestic point} \quad (8)$$

Note that the entire post-processing can also be conducted in the wavelengths domain. In this case, linear coefficients are given by other values than those calculated in the wavenumbers domain. These coefficients in the wavelengths domain are given at the end of section 3.

3. Results and Discussion

In this section, discussion will be proposed together with the presentation of the experimental results.

3.1. Determination of the Linear Coefficient and Position of the Isosbestic Point

The method described above was used with data obtained from the supplier's website [15] in order: first to demonstrate the linear evolution of the emitted energy, second to calculate the linear coefficients and their dependence with respect to the excitation wavelength and third to express the position of the isosbestic point as a function of the excitation wavelength.

Figure 2 shows the evolution of the emission energy as a function of pH for the 3 excitation wavelengths available in the supplier's website [15]. The top part shows the normalized energies calculated from the spectra according to equations (2) and (3). The bottom part shows the normalized energies difference from the average value at each excitation wavelength and expressed in percentage.

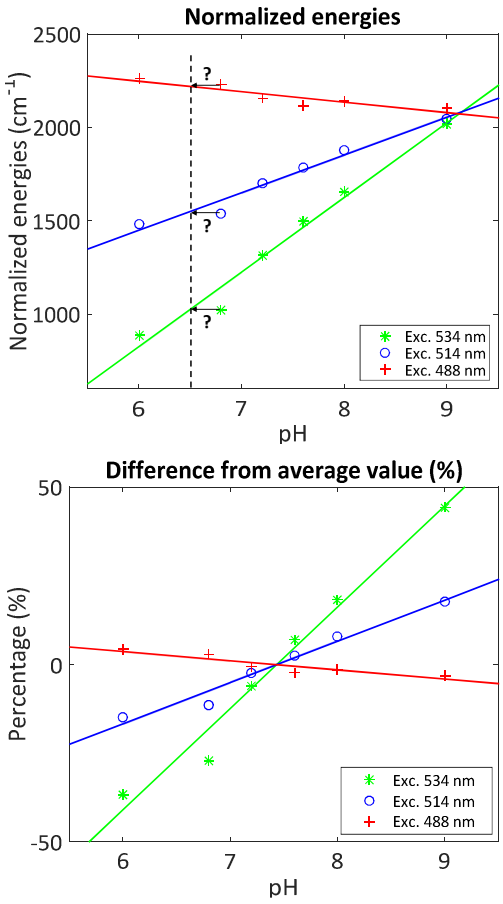

Figure 2. *Evolution of the normalized energies with pH for three excitation wavelengths. Data from supplier [15].*

The linear evolution of normalized energies with pH is clearly observed. There is a little question concerning result obtained for pH = 6.8. The linear regression would have been better with a solution at pH = 6.5 as indicated with question marks on the figure. However, calculations conducted using pH = 6.5 instead of pH = 6.8 does not significantly modify the coefficients of the linear regression.

The data obtained with an excitation wavelength of 488

nm show dispersion around the linear regression (especially at pH 7.2 and 7.6). This is due to two concomitant factors. First, the normalized energy evolves quite slowly when C-SNARF-1 is excited at 488 nm wavelength. The global variation in terms of percentage is +/- 5% over the pH range while it is over +/- 20% for an excitation at 514 nm and over +/- 50% for an excitation at 534 nm. Second, digitalization is somehow inaccurate, especially when the original data are represented with relatively thick lines. Those factors together explain why the dispersion of data is a bit larger excitation at 488 nm.

From these data, we can express the linear coefficients for each excitation wavelength. Data, calculated in the wavenumbers domain, are summarized in table 1.

Table 1. *Linear coefficients as a function of the excitation wavelength (in the wavenumbers domain).*

λ_{ex} (nm)	a (cm^{-1}. pH $unit^{-1}$)	b (cm^{-1})
534	399.6	-1571
514	201.7	238.5
488	-56	2583.6

Figure 3 shows the evolution of parameters "a" and "b" (top) and the position of the isosbestic point (bottom) as a function of the excitation wavelength. The linear behavior is clearly visible. Coefficients in equation (7) and (8) can now be calculated.

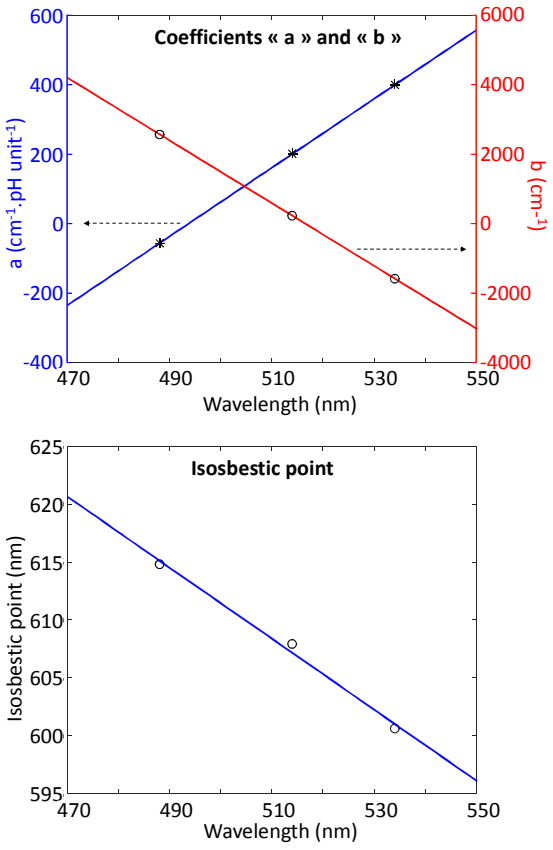

Figure 3. *Evolution of coefficients and isosbestic point as a function of the excitation wavelength. Top: coefficients "a" and "b". Bottom: position of the isosbestic point. Data from supplier [15].*

Table 2 summarizes the values of α, β and γ in equations (7) and (8) when calculated in the wavenumbers domain.

Table 2. *Coefficients α, β and γ.*

a	b	IB
$\alpha_1 = 9.904$ (cm^{-1} pH $unit^{-1}nm^{-1}$)	$\beta_1 = -90.31$ ($cm^{-1}nm^{-1}$)	$\gamma_1 = -0.307$
$\alpha_2 = -4889.3$ (cm^{-1} pH $unit^{-1}$)	$\beta_2 = 46656$ (cm^{-1})	$\gamma_2 = 764.7$ (nm)

3.2. Re-Calibration of Fluorescence Spectra

The post-processing was experimented with supplier's data, our own data and data from literature [23]. We also studied spectra given in [12] and discussed aspects concerning the position of the isosbestic point and excitation wavelength.

In order to test our method, amplitudes of the spectra from supplier presented in figure 1 were randomized. Post-processing is used to re-calibrate these artificially modified spectra. The result is given in figure 4. Modified supplier's data are represented on the top while re-calibrated spectra are given at the bottom. This re-calibration was performed considering an excitation wavelength of 488 nm. The isosbestic point is easily recovered after re-calibration.

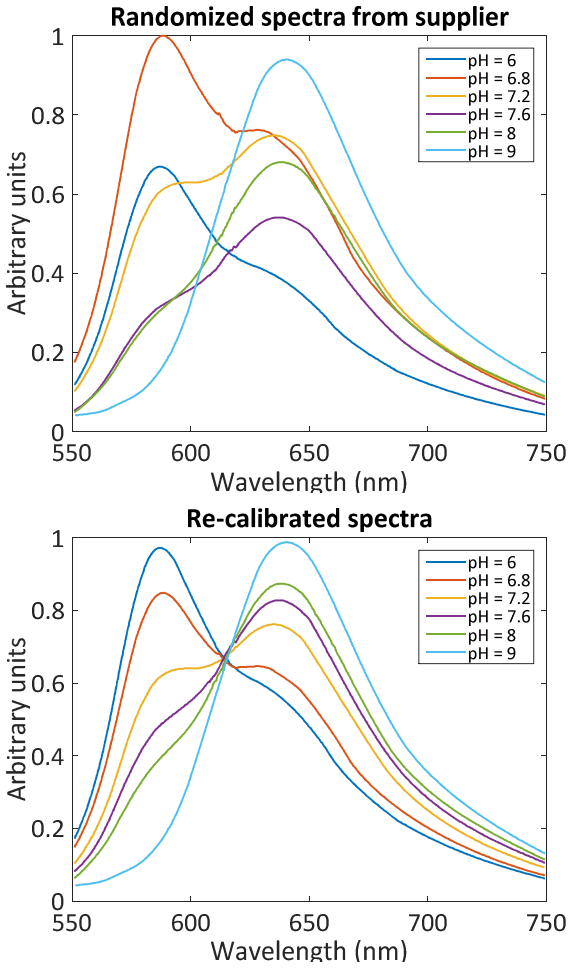

Figure 4. *Re-calibration using modified supplier's data.*

We next tested the method with our own data. The result is

given in figure 5. Our raw data are represented on the top while the re-calibration is shown at the bottom. It can be seen from this figure that experimentally, the spectra we recorded cannot be used for calibration. Buffer solutions containing C-SNARF-1 were prepared with extreme attention. Variations of the amplitudes of our spectra is mainly due to variations of excitation and collection. Indeed, we used very basic plastic cuvettes which are not sold for calibration purpose but more likely for qualitative measurements. Variations in the thickness of the plastic walls and path lengths may occur. More importantly, cuvettes were placed manually against the output SMA connector of the fluorescence beam-splitter. Between consecutive measurements, cuvettes were probably not always perfectly perpendicular to the optic axis of the beam-splitter. This results in variable path lengths and multiple reflection inside the cuvette which cannot be controlled. This is the main reason to the aspect of our raw data. However, it can easily be seen that the re-calibration method perfectly works. In this experiment, the excitation wavelength was 485 nm. Correction coefficients were computed from equation (7). Zooming around the isosbestic point shows that its re-calibrated position is around 614 nm, quite close to the 616 nm theoretical value given by equation (8) for this excitation wavelength.

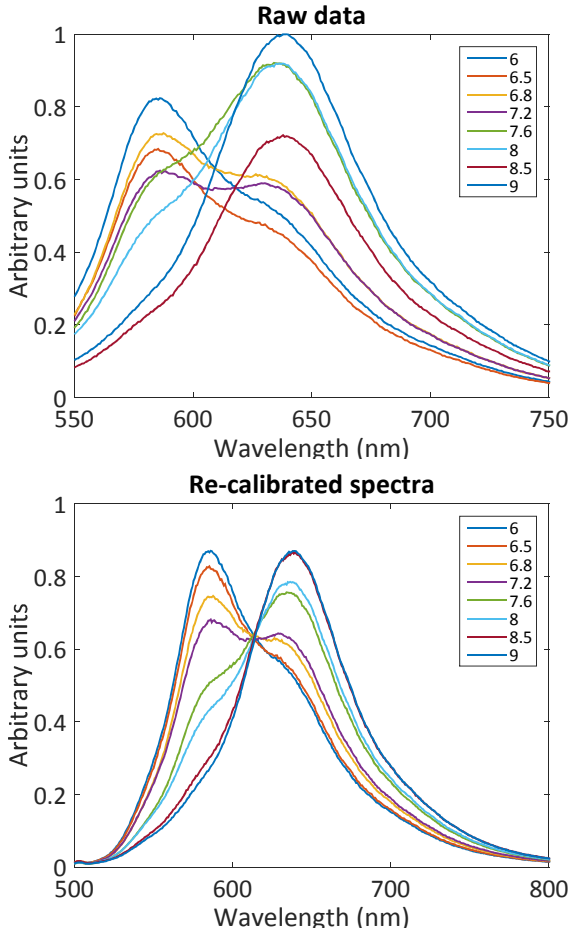

Figure 5. *Re-calibration using our own data. Top: raw data. Bottom: re-calibrated spectra.*

Then, we tested the method on data digitalized from [23]. The result is shown in figure 6. It can be seen that the isosbestic point is relatively well retrieved at a value around 614 nm in complete accordance with the value calculated from equation (8) for an excitation at 488 nm. However, re-calibration seems to be less efficient than it was for our own data. We think it is due to the difficulty to accurately digitalize data. Also, for our data, re-calibration was made considering the whole spectrum from 348 nm to 1127 nm which was not the case for digitalized data. Calculation of the energy with truncated data may induce uncertainty in the result.

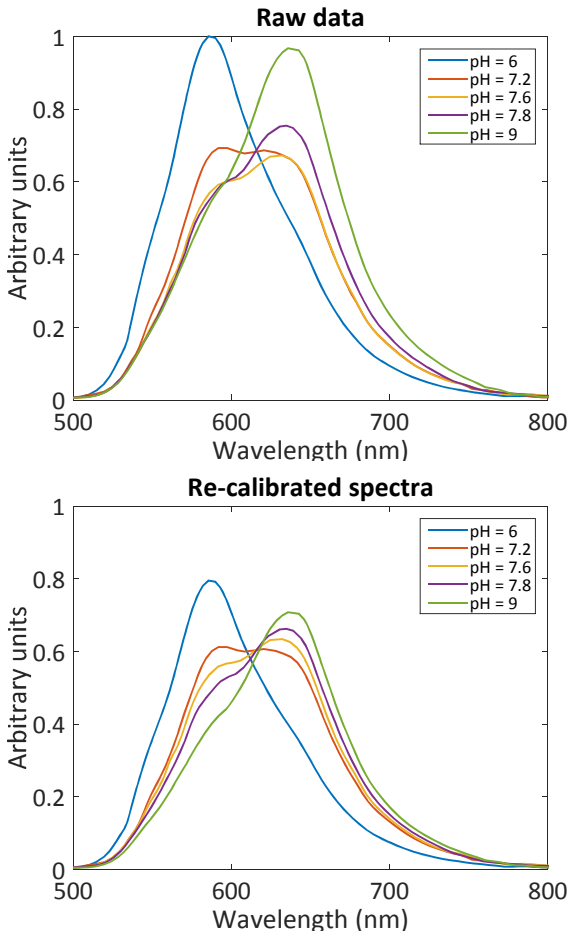

Figure 6. *Re-calibration using data digitalized from [23]. Top: raw data. Bottom: re-calibrated spectra.*

Finally, we analyzed the spectra given in [12] where an isosbestic point at 620 nm wavelength is observed for an excitation wavelength of 488 nm. This is not directly in accordance with what is mentioned above. However, this changes absolutely nothing to the numerical analysis of the spectra proposed in [12] where the spectra analysis is performed in order to account for the small number of free H^+ ions in the yeast mitochondria. It is possible that the internal medium of yeast slightly shifts the isosbestic point.

Data were analyzed according to our method. We found a=-323.5 and b=4274. According to equations (7), this corresponds to an excitation wavelength of 461 nm in terms

of coefficient "a" and 469 nm in terms of coefficient "b". Now using equation (8), these two wavelengths lead to an isosbestic point between 621 nm and 623.5 nm which is in accordance with the observed value. However, the numerical treatment proposed in this work makes the result independent of the value of the excitation wavelength or position of the isosbestic point.

More generally, our post-processing proved to be extremely efficient. We already mentioned the difficulties related to the poor accuracy of digitalization and truncation of the spectral data. Assessing the accuracy of this method is extremely difficult. Using the curve fitting toolbox in Matlab® to estimate uncertainties in the determination of coefficients "a" and "b" is not an option. The very small number of data with the different excitation wavelengths available (3 indeed) leads to large uncertainty despite the good linear regression we obtained in figures 2 and 3. At this level of development, the best way to assess the accuracy of the method is to visually evaluate the area into which the isosbestic point can be located, before and after re-calibration.

Before to conclude, table 3 shows the main parameters a, b, α and β when the calibration is conducted in the wavelengths domain.

Table 3. *Main parameters when the re-calibration is conducted in the wavelength domain.*

λ_{ex} (nm)	a	b (nm)
534	0.851	71.75
514	9.426	-8.03
488	16.401	-70.26
α and β	$\alpha_1 = 0.3376$ (nm^{-1}) $\alpha_2 = -164$	$\beta_1 = -3.09$ $\beta_2 = 1578$ (nm^{-1})

4. Conclusion

In this paper, we have presented a simple method to post-process fluorescence spectra used to calibrate C-SNARF-1 indicator for ratiometric pH measurements. A model describing the evolution of the emitted energy as a function of pH and excitation wavelength was proposed. We showed that the emitted energy evolves linearly with pH and we expressed this linear evolution as a function of the excitation wavelength. We also showed the evolution of the isosbestic point as a function of the excitation wavelength. The method was successfully applied to artificially modified spectra digitalized from the manufacturer's website. It was also successful in re-calibrating our own spectra and spectra digitalized from literature.

This post-processing considerably simplify indicators calibration procedures as calibration becomes independent of the indicator's concentration and path length and is not equipment dependent anymore. This method can easily be transposed to other ratiometric pH indicators exhibiting a dual emission peak and also more generally to ion sensing fluorescent indicators exhibiting dual emission peaks and for which the same initial calibration procedure is recommended. It is possible that the equations describing the fluorescence properties of other indicators exhibit a nonlinear behavior. Because re-calibration simply consists in multiplying normalized spectra by these equations, this post-processing remains valid regardless of the spectral behavior of the indicator.

References

[1] J. Han and K. Burgess, "Fluorescent Indicators for Intracellular pH", Chem. Rev., Vol. 110, Issue 5, pp 2709–2728, 2010. doi: 10.1021/cr900249z.

[2] J. Chao, Y. Liu, J. Sun, L. Fan, Y. Zhang, H. Tong and Z. Li, "A ratiometric pH probe for intracellular pH imaging", Sensors and Actuators B: Chemical, Vol. 221, Issue 31, pp. 427-433, 2015. dx.doi.org/10.1016/j.snb.2015.06.087.

[3] W. J. Zhang, L. Fan, Z. B. Li, T. Ou, H. J. Zhai, J. Yang, C. Dong and S. M. Shuang, "Thiazole-based ratiometric fluorescence pH probe with large Stokes shift for intracellular imaging", Sensors and Actuators B: Chemical, Vol. 233, pp. 566-573, 2016. dx.doi.org/10.1016/j.snb.2016.04.122.

[4] L. Ferrari, L. Rovati, P. Fabbri, and F. Pilati, "Disposable Fluorescence Optical pH Sensor for Near Neutral Solutions", Sensors, Vol. 13, pp 484-499, 2013. doi: 10.3390/s130100484.

[5] K. P. Dobmeier, G. W. Charvilleand M. H. Schoenfisch, "Nitric Oxide-Releasing Xerogel-Based Fiber-Optic pH Sensors". Analytical chemistry. Vol. 78, Issue 21, pp. 7461-7466, 2006. doi: 10.1021/ac060995p.

[6] M.-R. S. Fuh, L. W. Burgess, T. Hirschfeld, G. D. Christian and F. Wang, "Single fibre optic fluorescence pH probe", Analyst, Vol. 112, pp 1159-1163, 1987. doi: 10.1039/AN9871201159.

[7] I. Kasik, J. Mrazek, T. Martan, M. Pospisilova, O. Podrazky, V. Matejec, K. Hoyerova and M. Kaminek, "Fiber-optic pH detection in small volumes of biosamples", Anal Bioanal Chem Vol. 398, pp 1883–1889, 2010. doi 10.1007/s00216-010-4130-9.

[8] H. Diehl and R. Markuszewski, "Studies on fluorescein—VII", Talanta, Vol. 36, Issue 3, pp. 416-418, 1989. doi. org/10.1016/0039-9140 (89)80213-9.

[9] M. Yassine, J. M. Salmon, J. Vigoand P. Viallet, "C-SNARF-1 as a pHi fluoroprobe: discrepancies between conventional and intracellular data do not result from protein interactions", Journal of Photochemistry and Photobiology B: Biology, Vol. 37, Issue 1, pp 18-25, 1997. doi. org/10.1016/S1011-1344 (96)07339-3.

[10] B. Valeur, "Molecular Fluorescence: Principles and Applications". 2001 Wiley-VCH Verlag GmbH. ISBNs: 3-527-29919-X (Hardcover); 3-527-60024-8 (Electronic).

[11] J. E. Whitaker, R. P. Haugland and F. G. Prendergast, "Spectral and photophysical studies of benzo[c]xanthene dyes: Dual emission pH sensors", Analytical Biochemistry, Volume 194, Issue 2, pp. 330-3441991. doi. org/10.1016/0003-2697 (91)90237-N.

[12] T. M. Żurawik, A. Pomorski, A. BelczykCiesielska, G. Goch, K. Niedźwiedzka, R. Kucharczyk A. Krezel and W. Bal, " Revisiting Mitochondrial pH with an Improved Algorithm for Calibration of the Ratiometric 5 (6)-carboxy-SNARF-1 Probe Reveals Anticooperative Reaction with H+ Ions and Warrants Further Studies of Organellar pH", PLoS ONE 11 (8): e0161353, 2016. doi: 10.1371/journal. pone.0161353.

[13] K. J. Buckler and R. D. Vaughan-Jones, Application of a new pH-sensitive fluoroprobe (earboxy-SNARF-1) for intracellular pH measurement in small, isolated cells, Plügers Archiv, Vol. 417, pp. 234-239, 1990. doi: 10.1007/BF00370705.

[14] J. Bond, J. Varley, "Use of flow cytometry and SNARF to calibrate and measure intracellular pH in NS0 cells", Cytometry, 64A: 43–50. doi: 10.1002/cyto.a.20066.

[15] https://www.thermofisher.com/fr/fr/home/references/molecular-probes-the-handbook/ph-indicators/probes-useful-at-near-neutral-ph.html.

[16] A. C. Ribou, J. Vigo and J. M. Salmon, "C-SNARF-1 as a fluorescent probe for pH measurements in living cells: two-wavelength-ratio method versus whole-spectral-resolution method", J. of Chem. Educ., Vol. 79, Issue 12, pp. 1471-1474, 2002.

[17] M. L. Graber, D. C. DiLillo, B. L. Friedman and E. Pastoriza-Munoz, "Characteristics of fluoroprobes for measuring intracellular pH", Analytical Biochemistry, Vol. 156, pp. 202-212, 1986. dx.doi.org/10.1016/0003-2697(86)90174-0.

[18] F. Bancel, J. Vigo, J. M. Salmon and P. Viallet, "Acid—base and calcium-binding properties of the fluorescent calcium indicator indo-1", Journal of Photochemistry and Photobiology A: Chemistry, Vol. 53, Issue 3, pp. 397-409, 1990. dx.doi.org/10.1016/1010-6030(90)87142-X.

[19] A. K. Mahapatra, S. K. Manna, C. D. Mukhopadhyay and D. Mandal, "Pyrophosphate-selective fluorescent chemosensor based on ratiometric tripodal-Zn (II) complex: Application in logic gates and living cells", Sensors and Actuators B: Chemical, Vol. 200, pp. 123-131, 2014. dx.doi.org/10.1016/j.snb.2014.04.034.

[20] D. H. Kim, J. Seong, H. Lee and K. H. Lee, "Ratiometric fluorescence detection of Hg (II) in aqueous solutions at physiological pH and live cells with a chemosensor based on tyrosine", Sensors and Actuators B: Chemical, Vol. 196, pp. 421-428, dx.doi.org/10.1016/j.snb.2014.02.029.

[21] G. Grynkiewicz, M. Poenie and R. Y. Tsien, "A new generation of Ca^{2+} indicators with greatly improved fluorescence properties", The journal of biological chemistry, Vol. 260, Issue 6, pp. 3440-3450, 1985.

[22] P. A. Negulescu and T. E. Machen, "Intracellular ion activities and membrane transport in parietal cells measured with fluorescent dyes", Methods Enzymol., Vol. 192, pp. 38-81, 1990. doi: 10.1016/s1046-2023(05)80145-8. PMID: 2074799.

[23] D. Bottenus, Y. J. Oh, Sang M. Han, Cornelius and F. Ivory, "Experimentally and theoretically observed native pH shifts in a nanochannel array", Lab Chip, Vol. 9, pp. 219-231, 2009. doi: 10.1039/b803278e.